Journal of Solid State Chemistry **146,** 22–35 (1999)
Article ID jssc.1999.8296, available online at http://www.idealibrary.com on IDEAL®

Revisiting a Rare Intermetallic Ternary Nitride, Ni_2Mo_3N: Crystal Structure and Property Measurements

K. S. Weil,* P. N. Kumta,*,[1] and J. Grins†

*Department of Materials Science and Engineering, Carnegie Mellon University, Pittsburgh, Pennsylvania 15213; †Department of Inorganic Chemistry, Stockholm University, S-106 91 Stockholm, Sweden

Received October 30, 1998; received in revised form March 16, 1999; accepted March 23, 1999

The intermetallic ternary nitride, Ni_2Mo_3N, has been synthesized by the ammonolysis of a complexed mixed-metal chloride precursor. This compound crystallizes in the cubic space group $P4_132$ [213] with $Z = 4$ and a lattice parameter of $a = 6.6340(2)$ Å, as determined from powder X-ray and neutron diffraction experiments and the Rietveld refinement of the neutron data collected at room temperature. The refinement converged with $R_{wp} = 0.032$, $R_p = 0.025$, $R_I = 0.059$, and $\chi^2 = 1.48$. Ni_2Mo_3N assumes a filled β-manganese structure, ideally consisting of a lattice of corner-sharing Mo_6N octahedra in a five-membered ring arrangement and an interpenetrating net-like lattice of nickel atoms which occupy the pentagonal holes formed by the molybdenum nitride polyhedral rings. Electrical and magnetic characterization of Ni_2Mo_3N indicate that it is a metallic conductor which antiferromagnetically orders at 14.7 K. Neutron diffraction conducted at 10 K suggests that the size of the magnetic unit cell matches that of the crystallographic unit cell. A version of this nitride phase which is substoichiometric in nitrogen and therefore has a smaller lattice parameter also displays antiferromagnetic ordering, but with a much higher ordering temperature of 68.7 K. © 1999 Academic Press

INTRODUCTION

Historically, nearly all of the known ternary compounds that contain only transition metal elements and nitrogen can be classified by their crystal structure into one of two categories, either: (1) cubic, metallic perovskite structures, such as Fe_3NiN (1), or (2) cubic, η-carbide type structures such as Cr_3Ta_3N (2). Recently, a third structural type has come into existence, the hexagonal or rhombohedral layered structures, in which there are nine known members, including $MnWN_2$ (3) and $MnMoN_2$ (4). The constituent compounds of a fourth category, the cubic, π-phase structure which is better known as the filled β-manganese structure, can typically be described by a M_2T_3X stoichiometry, where M generally refers to a posttransition metal, T is a transition metal, and X is carbon or nitrogen. However, there are a handful of cases in which the compound consists of a mixture of transition metal elements, along with carbon or nitrogen. These are known to exist in the Fe–Cr–Mo–C and Fe–Cr–W–C (5) systems, although the exact ratios of the transition metal elements in these compounds have not been determined.

Goldschmidt (5) and Kuo (6) were the first to report finding new multicomponent transition metal carbide phases with the filled β-manganese structure. Initially observed as precipitates in tungsten strengthened stainless steels, the nominal composition of the compound was estimated to be $Fe_{10}Cr_9W_2C$ and was given the designation π-phase (6). Based on Kuo's work, it was immediately realized that other alloy compositions were likely to contain carbide and nitride precipitates with the filled β-manganese structure. However, it was not until the defining crystallographic work of Jeitschko, Nowotny, and Benesovsky (7,8) on a number of M–T–X systems (in which M is a Group IIIA element, T is a transition metal, and X is interstitial C or N) that the precise composition of these compounds was demonstrated to be M_2T_3X. Recently, Ono *et al.* (9) have reported observing a new π-phase nitride, Ni_2Cr_3N, in chromium-based tool steels, but did not pursue isolating the precipitates for further analysis. Although it has been suggested that the existence of these π-structured carbides and nitrides potentially has an important role in defining the carbon and nitrogen contents of austenitic stainless steels (10), the body of information on this family of compounds is very thin. In fact, in recently constructing the constitutional diagrams of the quaternary Fe–Cr–Ni–N and the quinary Fe–Cr–Ni–Mo–N systems, Hertzman (11) and Frisk (12) were forced to omit the π-phase compounds because of the limited thermodynamic and compositional data for these equilibrium phases.

Ni–Mo–N alloys with the β-manganese structure were first investigated by Evans and Jack in 1957 (13). The characteristic π-phase nitride, Ni_2Mo_3N, was later obtained by Nutter, Grieveson, and Jack in 1969 (14). They found

[1]To whom correspondence should be addressed.

0022-4596/99 $30.00

that the X-ray diffraction pattern of this phase was similar in appearance to Jeitschko's M_2T_3X compounds. Details of the nitride's crystal structure, such as atomic parameters and bond distances, however, were not reported. In an effort to determine the potential of Ni_2Mo_3N for application in cutting tools, Carr and Jack investigated its oxidation resistance and hardmetal properties (15). Very recently Herle *et al.* have reported on the synthesis and structure of this compound (16) and their X-ray diffraction work verifies that the compound crystallizes in a filled β- manganese motif, as presumed by Jack *et al.* Additionally, Herle *et al.* found that the resistivity of Ni_2Mo_3N was metallic in nature and that it displays Pauli paramagnetic behavior down to 20 K. In the course of our exploration of ternary nitrides in the Ni–Mo–N system, Ni_2Mo_3N was repeatedly formed either as a minor or major phase in a number of compositionally different samples. In this paper, we provide a rigorous analysis of the crystal structure of Ni_2Mo_3N, based on both X-ray diffraction and neutron diffraction data and discuss the electrical and magnetic properties of this compound, in particular focusing on results obtained at low temperature.

EXPERIMENTAL

The synthesis procedure involves essentially two sequential reaction steps: (a) the formation of a solid precursor induced by reacting the two transition metal chloride species in an acetonitrile solution with triethylamine, followed by (b) the ammonolysis of the complexed precursor to yield the ternary nitride. This technique has proven to be useful in synthesizing a number of ternary transition metal nitrides, including $CrWN_2$ (17) and Fe_3W_3N (18).

Precursor Synthesis

All chemical manipulations were conducted in an argon filled glovebox (O_2 and $H_2O \leq 5$ ppm; vacuum atmospheres) or under a protective stream of ultra high purity (UHP) nitrogen unless otherwise noted. All glassware used was acid washed with NoChromix and oven dried prior to use. Approximately 4–10-g quantities of nickel dichloride hexahydrate, $NiCl_2 \cdot 6H_2O$ (Aldrich, 99.9999%), and molybdenum pentachloride, $MoCl_5$ (Aldrich, 99.9%), were dissolved in a 2:3 stoichiometric molar ratio, respectively, in HPLC grade acetonitrile (Fisher Scientific). As the acetonitrile was slowly added, the resulting solution began to fume slightly, likely forming HCl gas due to the reduction of the molybdenum chloride salt. $MoCl_5$ is known to undergo reduction in acetonitrile, forming an acetonitrile soluble adduct, $MoCl_4 \cdot 2CH_3CN$ (19). Once the chlorides were thoroughly dissolved, triethylamine (99 + %, Sigma) was added to the solution under vigorous stirring. The amount of triethylamine needed for the reaction was determined, assuming complete coordination of each transition metal species by triethylamine. Since the ensuing reaction of triethylamine is slightly exothermic, and a triethylamine hydrogen chloride by-product does evolve, the triethylamine was added at a moderately slow rate of approximately 20 ml/min.

The addition of triethylamine resulted in a nearly instantaneous reaction as evidenced by rapid changes in the color and viscosity of the acetonitrile solution and by the formation of a thick cloud of a light, white solid that was continually swept out of the reaction vessel by the flowing nitrogen. Initially a watery, dark transparent blue liquid, the mixed chloride solution changes to an opaque green color and becomes much thicker upon complexing with triethylamine. The mixture was then heated to evaporate off the acetonitrile, leaving behind a soft, dark green powder product. The only crystalline phase found in the powder, as determined by X-ray diffraction, was triethylamine hydrogen chloride, $N(C_2H_5)_3 \cdot HCl$, which characteristically is a white powder consisting of fine needle-shaped particles. Thus, the two metal species are apparently present as an amorphous phase intermixed with the crystalline organic amine hydrogen chloride by-product.

Ammonolysis and Pyrolysis

A short series of heat treatment experiments were conducted on the nickel–molybdenum precursor to observe the evolution of phases as a function of ammonolysis temperature. Samples of the powder precursor were weighed into high purity aluminum nitride crucibles and placed into a $2\frac{1}{2}$-inch diameter quartz flow-through tube furnace. The back end of the tube furnace was connected to a mineral oil bubbler and the front end was connected to the gas line. Prior to initiating the heat treatment, the tube was purged for 20 min with prepure nitrogen, then purged for another 10 min with ammonia gas. The powder samples were fired in electronic grade anhydrous ammonia (Matheson Gas) flowing at a rate of 120 ml/min using the following sequence of heat treatment conditions: (1) ramp from room temperature to 120°C at 5°C/min and hold at 120°C for 1 h; (2) ramp from 120°C to 250°C at 3°C/min and hold at 250°C for 4 h; (3) ramp from 250°C to the soak temperature at 2°C/min and hold at this temperature for 20 h; (4) allow the sample to furnace cool. The soak temperatures that were employed were 550, 650, 700, 750, 850, and 950°C. The adduct, $N(C_2H_5)_3 \cdot HCl$, obtained as a by-product sublimes at 245°C and was not observed in the X-ray patterns of any of the heat-treated samples.

Chemical and Structural Characterization

Each of the powder products formed by ammonolysis was examined by energy dispersive X-ray spectroscopy (EDS) using an EDAX, DX-4 analyzer to semiquantitatively

verify the ratio of the metal species. Quantitative chemical assay of the title compound was conducted by Galbraith Laboratories (Knoxville, TN). They employed inductively coupled plasma optical emission spectroscopy to determine the concentration of the metal species, combustion analyses to evaluate the nitrogen, carbon, and oxygen contents following the American Society for Testing and Materials standard ASTM D5373 (20), and using coulometric titration for particularly low concentrations of these species, and ion chromatography and capillary electrophoresis techniques to determine the chlorine level. A second estimate of the nitrogen content in Ni_2Mo_3N was conducted by heating the sample in flowing air in a Perkin-Elmer thermogravimetric analyzer (model TGS-2) at a rate of 5°C/min.

Cursory X-ray diffraction analyses on the ammonolyzed Ni–Mo products were carried out on a Rigaku theta-theta diffractomoter with graphite monochromated Cu$K\alpha$ radiation under the following step scan settings: 10°–70° range, 0.05° step size, and 2–s collection time. The sample which gave the most crystalline X-ray diffraction pattern was reexamined for structural analysis using two X-ray diffraction techniques and neutron diffraction. The first X-ray pattern, used for indexing and lattice parameter measurements, was generated with a Guinier–Hägg focusing camera using Cu$K\alpha_1$ radiation over a 2θ range of 0°–90° and silicon as an internal standard. The X-ray films were evaluated using the SCANPI film scanner system (21). The DICVOL (22) indexing program and the PIRUM (23) cell refinement program were used to determine the Bravais lattice and indexing sequence and to refine the lattice parameter for the compound. A second set of X-ray diffraction data, which was used for structural refinement, was collected on a STOE STADI/P diffractometer in symmetric transmission mode using germanium monochromated Cu$K\alpha_1$ radiation under the following step scan settings: 5°–130° 2θ range, 0.02° step size, and 325-s collection time.

Neutron diffraction data were collected, both at room temperature and 10 K, at the Swedish research reactor R2 in Studsvik. A double monochromator system [Cu(220)] was employed to give a wavelength of 1.470 Å. After collimation ($\alpha_1 = 10'$ and $\alpha_2 = 12'$), the neutron flux at the sample position was $10^6\ cm^{-2}s^{-1}$. The volume of the sample was approximately 3 cm^3 and was contained within a 9-mm diameter vandium tube. The instrument had an array of 10 detectors spaced 3.12° apart. All detectors scanned each point in 2θ, and the intensities measured by each were added. Statistical analysis of the different contributions to each observed step intensity showed no anomalies. Data were collected in 0.08° steps over a 2θ range of 5 to 140°.

Both the X-ray and the neutron diffraction data sets were refined independently using the Rietveld refinement program, FULLPROF (24). The profile shape was represented by the modified pseudo-Voigt function (25,26), with profile asymmetry introduced by employing a multiterm Simpson's rule integration (27). In addition to the profile, lattice, thermal displacement, and structure parameters, the zero-point shift, nine background parameters, the scale factor, and the molybdenum and nickel stoichiometries were also refined. Nitrogen stoichiometry was refined using the neutron data only. Atomic thermal displacements were assumed to be isotropic. Crystal structure graphics and geometric calculations were prepared using the Ca.R.Ine software (28).

The morphologies and microstructural features of the ammonolyzed powder products were examined by scanning electron microscopy and by high resolution transmission electron microscopy using an AMRAY 1810 microscope equipped with a Robinson backscatter detector and a JEOL 3010 HRTEM microscope, respectively. The Ca.R.Ine software package (28) was used to construct simulations of the expected electron diffraction patterns and to assess if these match the experimental data.

Electrical and Magnetic Characterization

Temperature-dependent four-probe resistance measurements of Ni_2Mo_3N were made on a sintered sample measuring 0.5 mm by 1.5 mm by 2 cm in size. The measurements were conducted over a temperature range of 1.5 to 300 K using an EM P13 DC picovoltage source, a Keithley 220 programmable current source, and a Hewlett-Packard 3458A multimeter. Magnetic data were collected on several powder samples using a Lake Shore Cryotronics 7130 weak-field a.c. susceptometer over a temperature range of 11 to 323 K in an applied field of 250 A/m at a frequency of 125 Hz. All data were corrected for the diamagnetic contribution of the sample holder.

RESULTS AND DISCUSSION

As seen in the series of diffractograms shown in Fig. 1, the thermal soak conditions of the Ni–Mo precursor strongly influence the type of products that are obtained. At 550°C, two phases form, nickel metal and nanophasic molybdenum nitride, MoN. A layered phase, suspected to be $(Ni_{0.8}Mo_{0.2})MoN_2$ (29), is observed at 650°C, but only in combination with nickel and MoN. The diffraction peaks that are attributable to the layered phase are the most intense in the sample heat-treated at 700°C. By 750°C, the intermetallic ternary nitride, Ni_2Mo_3N, has formed. At higher temperatures, Ni_2Mo_3N is the sole ternary phase and no signs of the layered $(Ni_{0.8}Mo_{0.2})MoN_2$ phase remain.

Semiquantitative analysis of the high temperature samples (750°C, 850°C, and 950°C) using EDS consistently gave Ni/Mo ratios which were in good agreement with the expected value of 0.667. Quantitative chemical analyses conducted on the Ni–Mo sample ammonolyzed at 850°C, given in Table 1, indicate that its average stoichiometry is $Ni_{1.85}Mo_3N_{1.04}$, slightly substoichiometric in nickel and

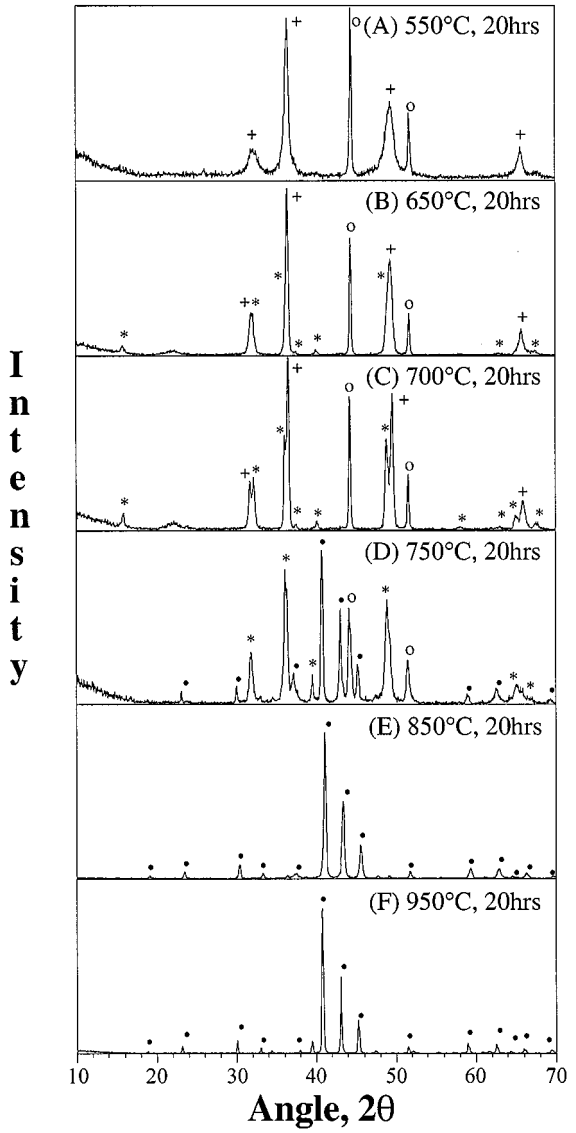

FIG. 1. X-ray diffraction patterns collected on Ni–Mo samples ammonolyzed at: (A) 550°C for 20 h, (B) 650°C for 20 h, (C) 700°C for 20 h, (D) 750°C for 20 h, (E) 850°C for 20 h, and (F) 950°C for 20 h. Peaks marked with an asterisk represent the layered phase, while those marked with a filled dot denote Ni_2Mo_3N. Peaks which can be attributed to the impurity phases MoN and nickel are represented by "+" and "○", respectively. The Mo_2N peaks in (E) and (F) are not marked.

slightly superstoichiometric in nitrogen relative to the π-phase stoichiometry of Ni_2Mo_3N. As will be seen from the X-ray and neutron diffraction data, there is a small amount of Mo_2N present as an impurity in this sample. It should be noted that all the impurities (O, C, Cl) that would normally be expected to be found in high levels in a product derived from this type of chemical synthesis approach are all relatively low in concentration (below 1000 ppm). Unlike the ternary alkali metal–transition metal nitrides and alkaline earth–transition metal nitrides, such as $NaTaN_2$ (30) and Ba_3FeN_3 (31), Ni_2Mo_3N appears to be quite stable to moisture and oxygen, as verified by the identical diffraction pattern and constant lattice parameters obtained, even after exposure of the compound to ambient atmosphere for several months.

The thermogram of this ammonolyzed sample when heated to 650°C in air indicates a maximum increase in weight of 38.8%, as shown in Fig. 2. As the sample is heated further to 700°C and beyond, it begins to rapidly lose weight, which is likely due to the sublimation of the MoO_3 that forms from the oxidation of the nitride at lower temperatures. NiO and MoO_3 were the only two phases identified in a subsequent X-ray diffraction analysis of this oxidized sample. The weight change observed in this experiment is in agreement with the results obtained from the quantitative chemical analyses. The Ni–Mo sample which was ammonolyzed at 950°C was also thermogravimetrically analyzed. When heated to 650°C in air, it displayed a 39.4% weight increase, suggesting that the ternary intermetallic nitride formed in ammonia at 950°C is substoichiometric in nitrogen by at least 11at.%. The significance of this nitrogen deficiency will become more apparent in the discussion on magnetic properties.

The X-ray pattern was indexed to a primitive cubic unit cell with a lattice parameter of $a = 6.6340(2)$ Å and systematic absences consistent with those of the $P4_132$ [213] space group. Since the lattice parameter and space group are similar to those reported by Jeitschko *et al.*, for M_2T_3X (7, 8), the atomic coordinates of this model were used as the starting point for Rietveld refinements of Ni_2Mo_3N. Once the crystal structure was refined, bond lengths for the various nearest neighbor combinations were calculated to determine the validity of the structure. A small amount of a second phase, determined to be Mo_2N, was observed in the diffraction patterns of the 850°C ammonolyzed sample. This impurity was initially refined using two different structural models. The first was the hexagonal structure of α-Mo_2C (32) with a space group of $P63/mmc$ and cell parameters of $a = 3.0078(1)$ and $c = 4.7401(3)$. The second was

TABLE 1
Chemical Analysis of the 850°C Ammonolyzed Ni–Mo Compound

Concentration (atom %)	Sample 1	Sample 2	Avg. calculated composition	Theoretical
Ni	31.40	31.17	31.29	33.33
Mo	50.93	50.72	50.83	50.00
N	17.34	17.83	17.59	16.67
C	0.16	0.10	0.13	
O	0.08	0.09	0.09	
Cl	0.06	0.04	0.05	

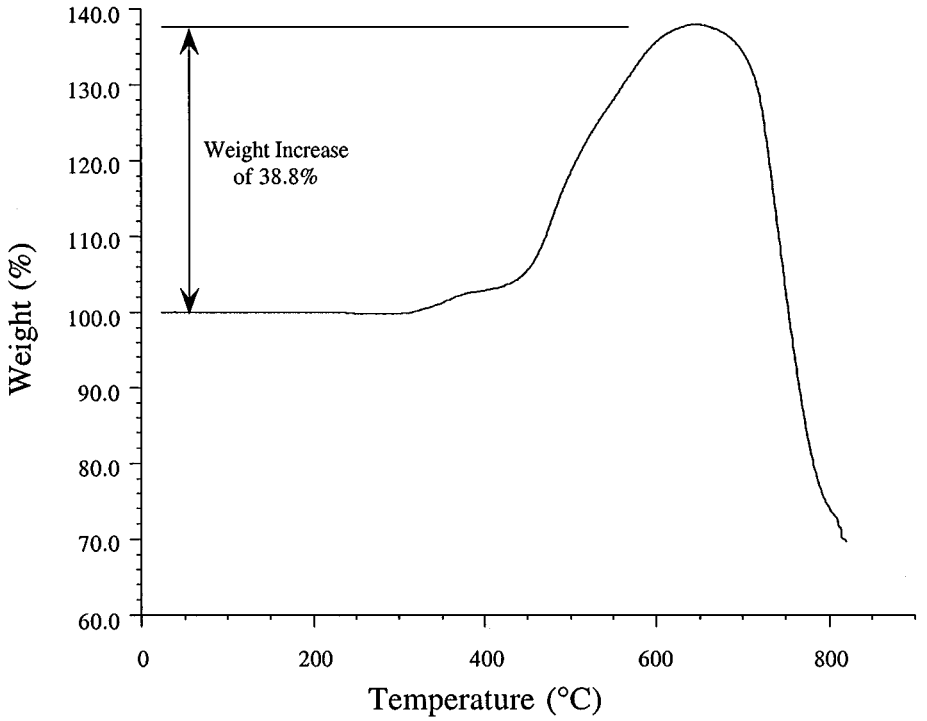

FIG. 2. Thermogravimmetric analysis of the Ni–Mo sample ammonolyzed at 850°C (nominally Ni_2Mo_3N) heated at 5°C/min to 820°C in air.

the newly discovered orthorthombic polymorph of Mo_2N, first reported by Marchand (33) which is argued to be isotypic with Mo_2C and crystallizes in the space group *Pbcm* with orthorhombic lattice parameters that correlate with the above hexagonal model, where the parameter $a = c_{hex}$, $b = 2a_{hex}$, and $c = 3a_{hex}$. Both models gave similar refinement results for our X-ray data, leading us to choose the simpler hexagonal model for the later neutron refinements.

The data for both the impurity phase and the ternary nitride were simultaneously refined, converging with the following residuals for the entire pattern: $R_{wp} = 0.074$, $R_p = 0.056$, $D_{wd} = 1.10$, and $\chi^2 = 1.04$. The residuals for each phase were $R_I = 0.025$ and $R_F = 0.025$ for the 68 reflections of the Ni_2Mo_3N phase and $R_I = 0.059$ and $R_F = 0.044$ for the 21 reflections of the Mo_2N phase. The atoms in Ni_2Mo_3N were found to be distributed over the following Wyckoff positions in the $P4_132$ space group: 1 Ni in 8(c) at (0.0671[2], 0.0671[2], 0.0671[2]), 1 Mo in 12(d) at ($\frac{1}{8}$, 0.2016[1], 0.4516[2]), and 1 N in 4(a) at ($\frac{3}{8}$, $\frac{3}{8}$, $\frac{3}{8}$). Using the hexagonal model (space group: *P*63/*mmc*) for Mo_2N, the atom positions were found to be: 1 Mo at 2(c) at (1/3, 2/3, 1/4) and 1 N in 2(a) at (0,0,0). An initial estimate of the relative weight fractions of the two nitride phases was calculated from their respective scale factors. Accordingly, the 850°C ammonolyzed sample used for structural analysis was estimated to contain 93.1% Ni_2Mo_3N and 6.9% Mo_2N by weight. However, this estimate was revised for employment in later calculations by averaging it with the information from the chemical analyses, giving 94.3% Ni_2Mo_3N and 5.7% Mo_2N by weight.

Powder neutron diffraction data were collected on the 850°C ammonolyzed sample, both at room temperature and at 10 K, in order to verify the X-ray diffraction data and more importantly to reveal a possible magnetic ordering of the nickel atoms. Indexing of the room temperature neutron data was consistent with that of the X-ray data. The corresponding residual values for Rietveld refinement of the room temperature neutron diffraction data were: $R_{wp} = 0.032$, $R_p = 0.025$, $D_{wd} = 1.48$, and $\chi^2 = 1.48$ for the pattern fit, $R_I = 0.059$ and $R_F = 0.049$ for the 85 reflections of the Ni_2Mo_3N phase, and $R_I = 0.16$ and $R_F = 0.17$ for the 23 reflections of the Mo_2N phase. The atomic parameters obtained from this refinement agree extremely well with those from the X-ray refinement. The neutron data for the crystal structure of Ni_2Mo_3N and the results of this refinement and the atomic positions are reported in Table 2. Note that all three atom occupancies in Ni_2Mo_3N were refined to values of 1.0 in this analysis. Selected bond distances and angles are given in Table 3. Figure 3 shows a comparison of the experimental neutron diffraction plot collected at 295 K with that obtained by refinement, along with the calculated residuals. Figure 4 shows a model of the unit cell that is consistent with the Rietveld refinements and two sets of diffraction data.

TABLE 2
Results of the Rietveld Refinement for Ni_2Mo_3N in Space Group $P4_132$

Chemical formula	Ni_2Mo_3N
Formula weight	419.21
Crystal system	Cubic
Space group	$P4_132$
a (Å)	6.6340(2)
V (Å^3)	291.96(5)
Z	4
D_{calc} (g/cm^3)	9.541
Powder color	Dark gray
Neutron radiation	1.470 Å
Monochromator	Cu (220)
2θ range (°)	5.00–140.00
Scan step size (°)	0.08
Count time (s/step)	10
Test temperature (°C)	22 ± 1
No. of reflections	85
No. of profile parameters	21
No. of structure parameters	9
Reliability factors[a]	
R_{wp}	0.032
R_p	0.025
R_I	0.059
D_{wd}	1.48

Atomic Parameters for Ni_2Mo_3N

Atom	x	y	z	$100U_{iso}$ (Å^2)	Occupancy
Ni	0.0669(2)	0.0669(2)	0.0669(2)	0.422(7)	1.0(1)
Mo	1/8	0.2017(1)	0.4517(2)	0.386(9)	1.0(3)
N	3/8	3/8	3/8	0.871(1)	1.0(1)

[a]Defined: $R_{wp} = \{[\sum W_i(Y_{obs} - Y_{cal})^2/(\sum W_i(Y_{obs})^2]\}^{1/2}$; $R_p = (\sum | Y_{obs} - Y_{cal}|)/(\sum Y_{obs})$; $R_I = (\sum|I_{obs} - I_{cal}|)/(\sum I_{obs})$.

Electron diffraction studies verified the cubic structure of Ni_2Mo_3N, as well as the lattice parameter obtained from the Guinier–Hägg diffraction experiment, $a_{e.d.} = 6.7$ Å and $a_{G-H} = 6.6340(2)$ Å, respectively. Shown in the micrograph in Fig. 5a is a typical electron diffraction pattern of Ni_2Mo_3N, as viewed along the [012] zone axis. A simulation of the pattern, based on the data obtained from Rietveld refinement, is constructed in Fig. 5b and confirms the experimental pattern. An HREM image of two Ni_2Mo_3N crystallites joined along a common boundary is shown in Fig. 5c. Evidence of the cubic unit cell shape of Ni_2Mo_3N is apparent, particularly in the thin sections near the edges of each crystallite. An SEM image of the nitride taken at lower magnification, seen in Fig. 6, displays the cubic morphology of the Ni_2Mo_3N crystallites.

Ni_2Mo_3N crystallizes in an interstitial-filled version of the β-manganese structure, isostructural with that of Al_2Mo_3C (8). Among the pure transition metals, manganese is singular in several respects. First, it possesses a complex allotropic series of crystal structures, two of which, α- and β-manganese, are highly complicated, while the metals surrounding it in the periodic table all crystallize with simple structures. Second, because of the key position of maganese in the periodic table, intermediate to the iron and chromium group elements, it is possible for binary or ternary intermetallic compositions which do not contain manganese to form electron compounds which crystallize in one of these allotropic structures. Finally, manganese occupies a unique boundary position between strong and weak carbide- and nitride-forming elements. The crystal structure of β-manganese is known from the original work of Westgren and Phragmen (34). Two "types" of manganese atoms, as characterized by the differing Wyckoff positions and atomic bond distances, respectively, comprise 12 and 8 of the 20 metal atoms per unit cell. As Goldschmidt suggests, these two atom types also differ in their electronic states and in the ternary π-structured compounds offer sites inherently predisposed to occupation by atoms of different species (5). In the case of Ni_2Mo_3N, the nickel atoms occupy the 8(c) Wyckoff positions, the molybdenum atoms rest in the 12(d) sites, and the nitrogen atoms occupy the 4(a) sites.

Polyhedral representations of the atomic coordination in Ni_2Mo_3N consistent with the Rietveld refinement and diffraction data are displayed in Fig. 7a–c and 8a–d. As shown in Fig. 7a, the nitrogen atoms of this metal-rich compound are octahedrally coordinated by molybdenum, forming very slightly distorted NMo_6 octahedra. These octahedra share corners forming a three-dimensional network. When viewed along the $[32\bar{2}]$ direction, the corner-sharing NMo_6 octahedra of Ni_2Mo_3N, seen in Fig. 7b, appear to form five-membered rings, each containing a small pentagonal shaped hole. When viewed along the [320] direction, Fig. 7c, the ring is obviously not flat, but assumes an undulated conformation with three octahedra all pointing in one direction and two octahedra pointing in the other. Displayed separately in Fig. 8a, the nickel atoms also form a three-dimensional net-like structure in which each nickel atom is bonded to three adjacent nickel atoms. These three adjacent nickel atoms are coplanar, forming an equilateral triangle,

TABLE 3
Selected Bond Distances and Angles in Ni_2Mo_3N

Bond distances (Å)			Bond angles (°)		
Ni–Ni	2.468(9)	3×	Mo–N–Mo	85.1 (3)	2×
Ni–Mo	2.817(3)	3×	Mo–N–Mo	94.8(7)	2×
Ni–Mo	2.739(8)	3×	Mo–N–Mo	180.0(0)	3×
Ni–Mo	2.732(2)	3×	Mo–N–Mo	90.0(0)	8×
Ni–N	3.219(4)	3×	N–Mo–N	154.8(7)	2×
Mo–Mo	2.815(9)	4×	Mo–Ni–Mo	61.1(1)	3×
Mo–Mo	2.776(3)	2×	Ni–Mo–Ni	53.7(6)	2×
N–Mo	2.081(2)	6×	Ni–Ni–Ni	63.1(7)	3×
N–N	4.062(5)	5×	Ni–Ni–Ni	60.0(0)	3×

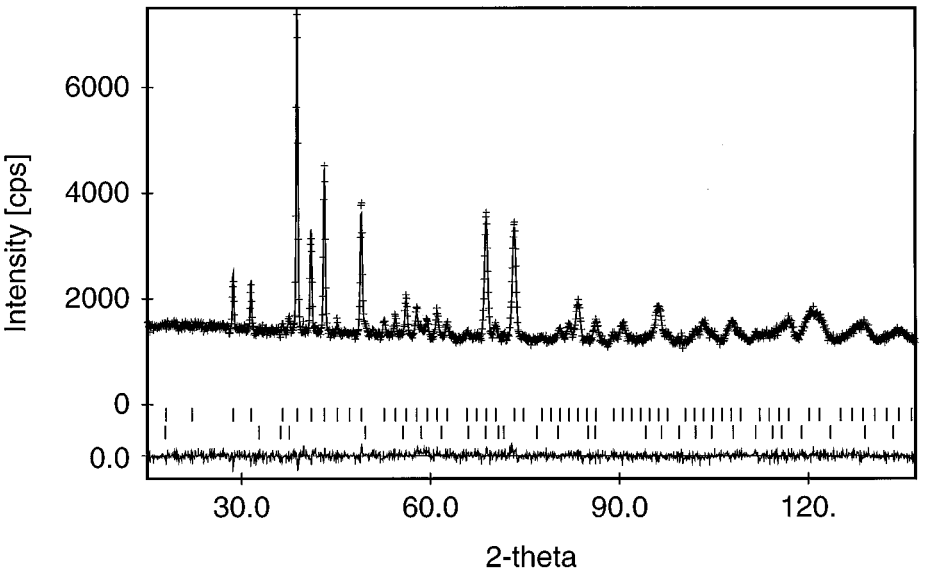

FIG. 3. The observed (crosses) and calculated (solid) neutron diffraction profile for Ni_2Mo_3N collected at 295 K. TiC marks below the diffractogram represent the allowed Bragg reflections. The residual line is located at the bottom of the figure.

Fig. 8b. The central nickel atom, however, does not quite lie in this plane, Fig. 8c, but is centered 0.4448 Å below it. This "fishing-net" lattice of nickel atoms interpenetrates within the interstices of the NMo_6 lattice structure, Fig. 8d.

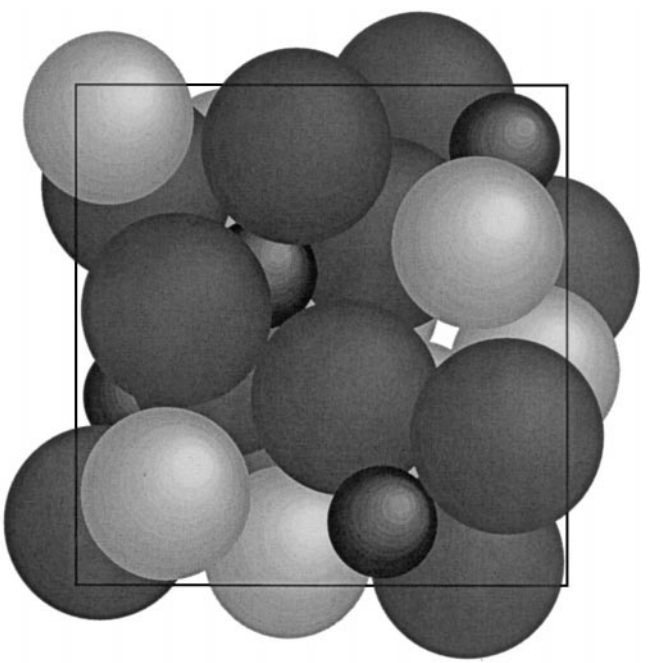

FIG. 4. The proposed unit cell structure of Ni_2Mo_3N. The dark gray, large spheres represent the molybdenum atoms; the light gray, medium size spheres represent the nickel atoms; and the small, dark gray spheres represent the nitrogen atoms.

The structure of Ni_2Mo_3N can be compared with that of the η-nitrides, the other cubic intermetallic nitride structure containing both early and late transition metal elements. While the unit cell of Ni_2Mo_3N is significantly smaller than that for the η-compounds, such as Ni_3Mo_3N (29), for example, which has a lattice parameter of 11.0995(2) Å, several features are common to both crystal structures. The first is that the early transition metal element, in this case molybdenum, forms octahedral clusters with nitrogen. Second, these NMo_6 octahedra share corners, forming a three-dimensional linked network. Finally, the nickel atoms in both structures also form their own separate network interwoven throughout the interstitial holes formed by the NMo_6 network.

There are two important structural differences, however, between Ni_2Mo_3N and Ni_3Mo_3N, that appear to lead to significantly different trends in the magnetic characteristics of the two materials. The NMo_6 corner sharing octahedra in the η-structure form rings which contain six octahedral members and a relatively large hexagonal space within each ring. On the otherhand, as seen in Fig. 7b, the corner-sharing NMo_6 octahedra of Ni_2Mo_3N form five-membered rings containing a much smaller pentagonal shaped hole. The nickel atoms in each compound also have a particular type of connectivity that is likely dictated by the NMo_6 network structure. In Ni_2Mo_3N, the net-like lattice of nickel atoms are formed by connecting each nickel atom directly to three others in a nearly trigonal planar arrangement. In Ni_3Mo_3N, the nickel atoms cluster into groups of eight, arranged into four tetrahedra, each which share a face with a fifth central tetrahedron, thus forming a stella

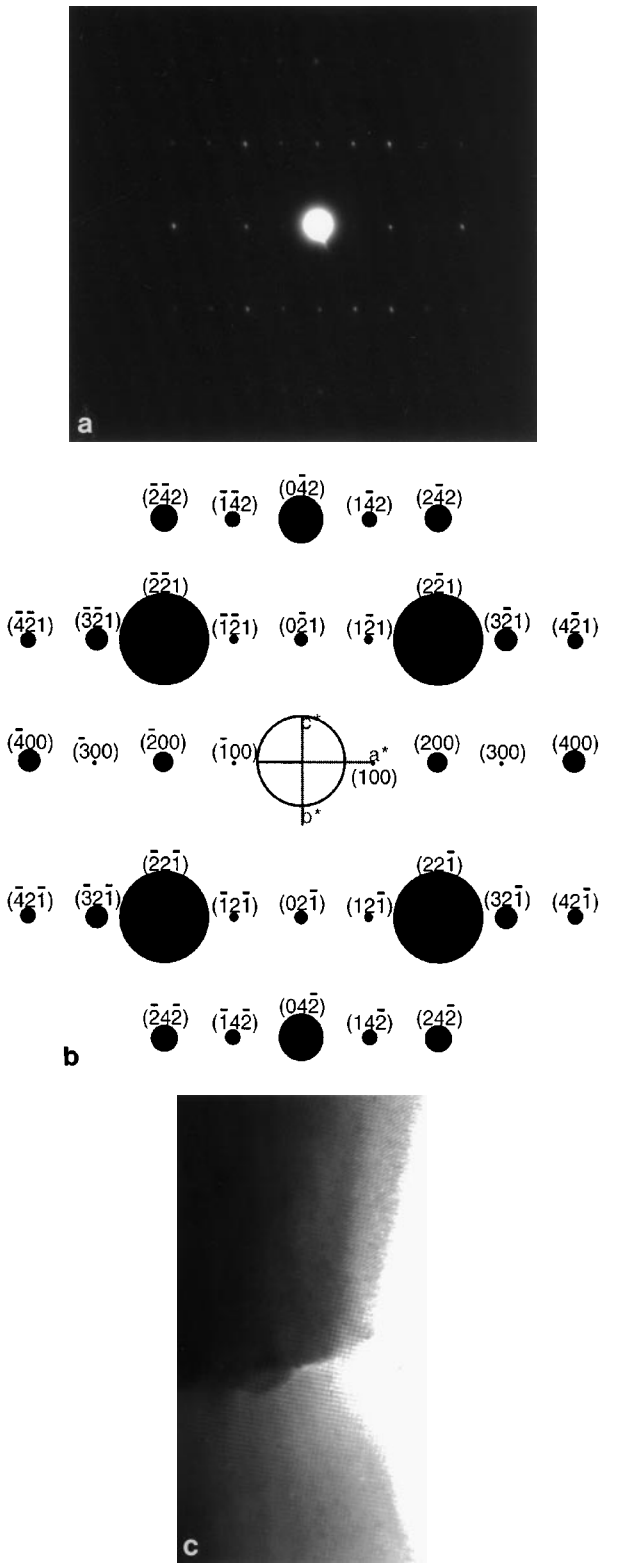

FIG. 5. (a) An electron diffraction image of Ni_2Mo_3N, as viewed down the [012] zone axis. The pattern indicates a primitive cubic cell with an approximate lattice parameter of $a = 6.7$ Å, which was confirmed by indexing the simulated diffraction pattern in (b). Shown in (c) is an HREM image of two Ni_2Mo_3N crystallites found in the 850°C ammonolyzed sample.

quadrangula (35). These Ni_8 stellae quadrangulae share corners, forming a connected three-dimensional lattice. Because the pentagonal interstices of Ni_2Mo_3N are smaller in size than the hexagonal holes of Ni_3Mo_3N, they cannot accommodate the large stellae quadrangulae that the η-structured nitride does. Instead, the nickel atoms in Ni_2Mo_3N assume the much simpler "net-like" structure seen in Figs. 8a and 8d. One consequence of these structural differences is that the magnetic behavior of these two intermetallic nickel molybdenum nitrides differs dramatically. As will be described below, Ni_2Mo_3N is antiferromagnetic, whereas Ni_3Mo_3N and other η-nitrides such as Co_3W_3N and Fe_3W_3N, are paramagnetic (29), approximately following the Curie–Weiss relationship over a 10–300 K temperature range.

The metal–metal and metal–nitrogen bond distances found in Ni_2Mo_3N are similar to those found in other intermetallic ternary transition metal nitrides. The Mo–N bond distance in Ni_2Mo_3N of 2.081(2) Å compares well with that for the Mo–N bond in Fe_3Mo_3N, 2.119(5) Å (36). Likewise, the Mo–Mo bond distances in Ni_2Mo_3N of 2.776(3) Å and 2.815(9) Å are similar to, though somewhat shorter, than those found in Co_3Mo_3C of 2.901(2) Å and 3.090(5) Å (37) and in Fe_3Mo_3N, 2.881(2) Å and 3.110(5) Å (36). The metal–nitrogen bond lengths in these ternary transition metal nitrides are significantly longer, by nearly 10–20%, in comparison to bond lengths existing in the alkali- and alkaline-earth-transition metal nitrides. The Mo–N bonds in Ni_2Mo_3N are also longer than the W–N bonds in the layered $CrWN_2$ and $FeWN_2$ structures by approximately 6.5%. The longer metal-nitrogen bond lengths imply that the bonding in Ni_2Mo_3N is at least partially covalent. When compared with metallic molybdenum, the Mo–Mo bond distance in Ni_2Mo_3N is nearly equivalent, suggesting that metallic bonding occurs between the molybdenum atoms within the NMo_6 octahedra. The Ni–Ni bond lengths in Ni_2Mo_3N are actually slightly shorter than those reported in metallic nickel, again implying that the nickel atoms form metallic bonds within their net-like lattice.

Four probe dc resistivity measurements carried out over a temperature range of 1.5 to 300 K were conducted on a densified bar of the 850°C ammonolyzed sample. The sample was prepared by cold pressing a 2.2-cm diameter pellet at 5000 psi using a hand press. The pellet was then heated at 925°C in a slowly flowing ammonia atmosphere for three days. Geometric density measurements indicate that the sample was approximately 95% dense. Posttesting X-ray diffraction analysis demonstrated that the pellet was essentially composed of Ni_2Mo_3N with a small amount of Mo_2N (estimated to be $\sim 6\%$ by weight). As seen in Fig. 9. between 49.8 and 300 K the resistivity of Ni_2Mo_3N displays a linear temperature dependence and a positive temperature coefficient of resistance, of $3.23 \times 10^{-9}\,\Omega \cdot m/K$, which is

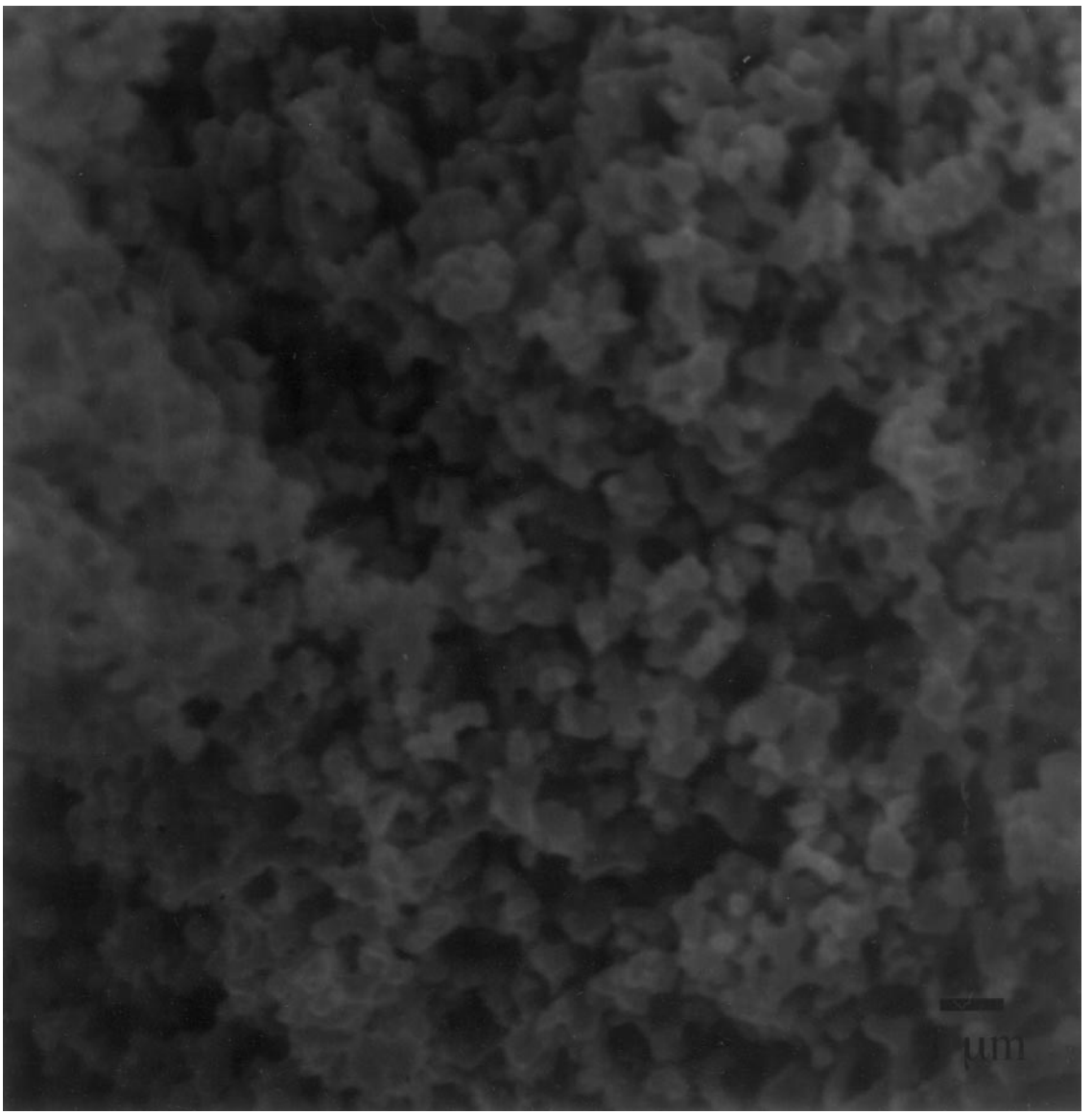

FIG. 6. An SEM micrograph displaying the cubic morphology of the Ni_2Mo_3N crystallites obtained after heat treatment of the precursor in flowing ammonia at 850°C for 20 h.

characteristic of metallic electrical behavior. In fact, the resistivity in this temperature range is relatively low and is comparable to that of a metallic conductor such as nichrome wire. Below 49.8 K, the resistivity curve changes slope, flattening until 5.9 K at which point a sharp decrease is observed. The change in slope at 49.8 K is likely due to an antiferromagnetic to paramagnetic transition, with $T_N = 49.8$ K. The lower temperature trend is indicative of a possible Meissner effect in the sample, although during testing, the temperature was never decreased to a point low enough that zero resistivity was observed. Interestingly, the related carbide, Al_2Mo_3C, which also crystallizes in the β-manganese structure, is a known superconductor with a critical temperature of $T_c = 10.0$ K (38) and a critical field of $H_c = 156$ kOe at 1.2 K (39). However, Mo_2N is also known to exhibit superconducting behavior (40). It may be possible that the resistivity drop at 5.9 K could be due to the dispersed Mo_2N impurity phase in our sample. Since this impurity could not be eliminated in our powders, it was not possible to test whether the dramatic drop in resistivity is attributable to the Ni_2Mo_3N or the Mo_2N phase.

The magnetic measurements were conducted on the as-ammonolyzed powders over a temperature range of 11 to 323 K, which unfortunately was not low enough to confirm indications of a Meissner phenomenon observed during the resistivity measurements. In all cases, susceptibility data

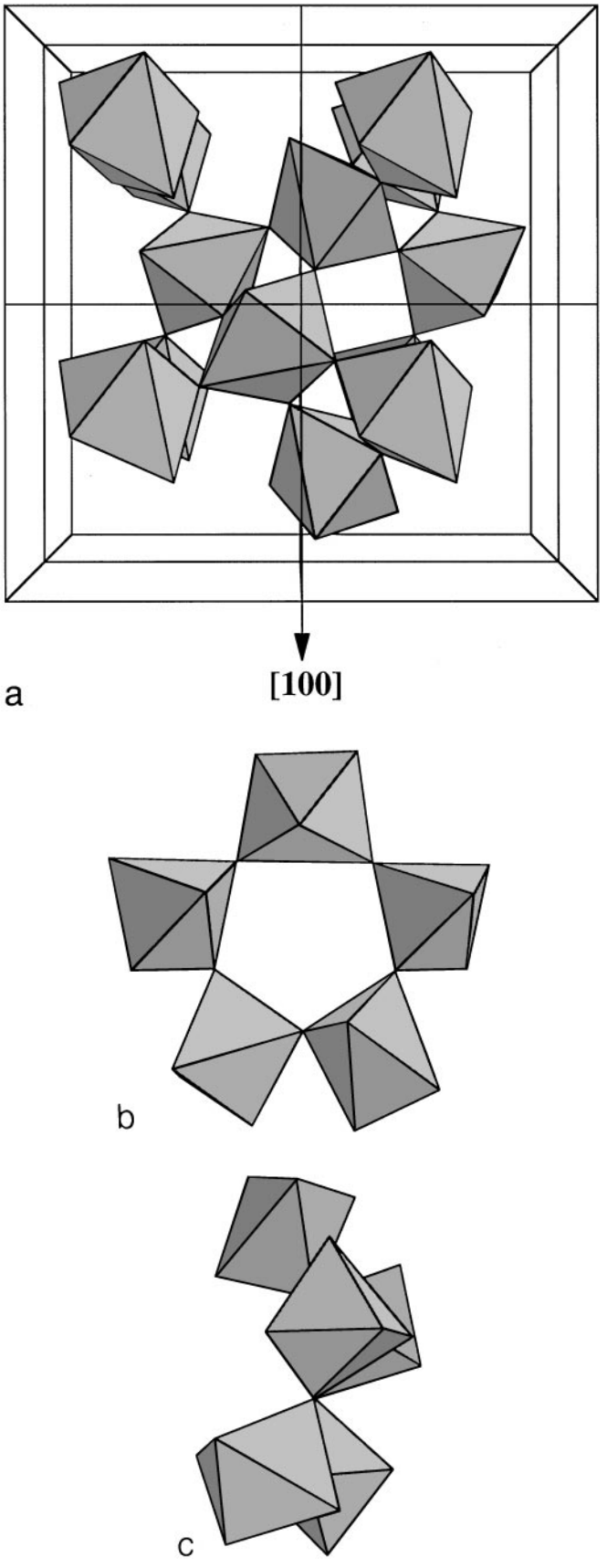

collected at different frequencies and magnetic fields yielded identical curves. Shown in Figs. 10a and b are the molar susceptibility and inverse molar susceptibility curves as a function of temperature for the 850°C heat treated Ni_2Mo_3N product. The sample displays a fairly well-defined antiferromagnetic ordering peak at 14.7 K and above that temperature the behavior appears to be paramagnetic. The fact that this T_N differs from that observed in the resistivity measurements may be due to an inadvertent loss of nitrogen from the compound that could have occurred during the thermal consolidation of the conductivity sample, as will be discussed in more detail below. A number of the metallic perovskites are also known to display antiferromagnetic behavior, including Mn_3GaC in which the spins on the manganese atoms are aligned opposed to each other in a collinear fashion (41) and Mn_3GaN, where the manganese spins assume a pure triangular antiferromagnetic mode (42). The neutron diffraction pattern on Ni_2Mo_3N recorded at 10 K was similar to the room temperature pattern. No additional super-cell reflections caused by magnetic ordering appeared in the low temperature pattern, suggesting that the size of the magnetic unit cell matches that of the crystallographic unit cell. There are some minor differences in the peak intensities between the two diffraction patterns, but any interpretations regarding these differences with respect to the magnetic structure of the compound would be speculative at this point.

Ni_2Mo_3N contains eight nickel atoms per unit cell. It is possible to regard the unit cell of this nitride as a combination of two sublattices of nickel atoms, by identifying those atoms which are coplanar with each other in sets of three and those which lie 0.4448 Å below these coplanar sets. With this in mind, a test was made to see whether the Néel equation for a two-sublattice antiferromagnet could be fitted to the susceptibility curve,

$$\frac{1}{\chi_M} = \frac{1}{C}\left[T - \theta_a - \frac{\theta_b^2}{T-\theta}\right], \qquad [1]$$

where $C = C_1 + C_2$, in which C_1 and C_2 are the Curie constant for the two sublattices; T is the absolute temperature; and θ_a, θ_b, and θ are the parametric temperatures defined by Goodenough in (43). Fitting Eq. [1] to the paramagnetic part of the curve yielded the following values for the constants: $C = 1.02(1)$ emu $\cdot K \cdot$ mol^{-1}, $\theta_a = -36.5(8)$ K, $\theta_b^2 = 0.1(5)$ K^2, and $\theta = 10.2(5)$ K. The fact that

FIG. 7. Polyhedral representations of the NMo_6 octahedra in the Ni_2Mo_3N structure. (a) displays the coordination of each nitrogen atom by six molybdenum atoms, forming NMo_6 octahedra which corner share. The corner-sharing arrangement of these octahedra into pentagonal rings is illustrated in (b) and (c). Note in (c) that the rings are not flat, but convoluted with two opposing octahedra pointing to the right in this side view and the other three pointing to the left.

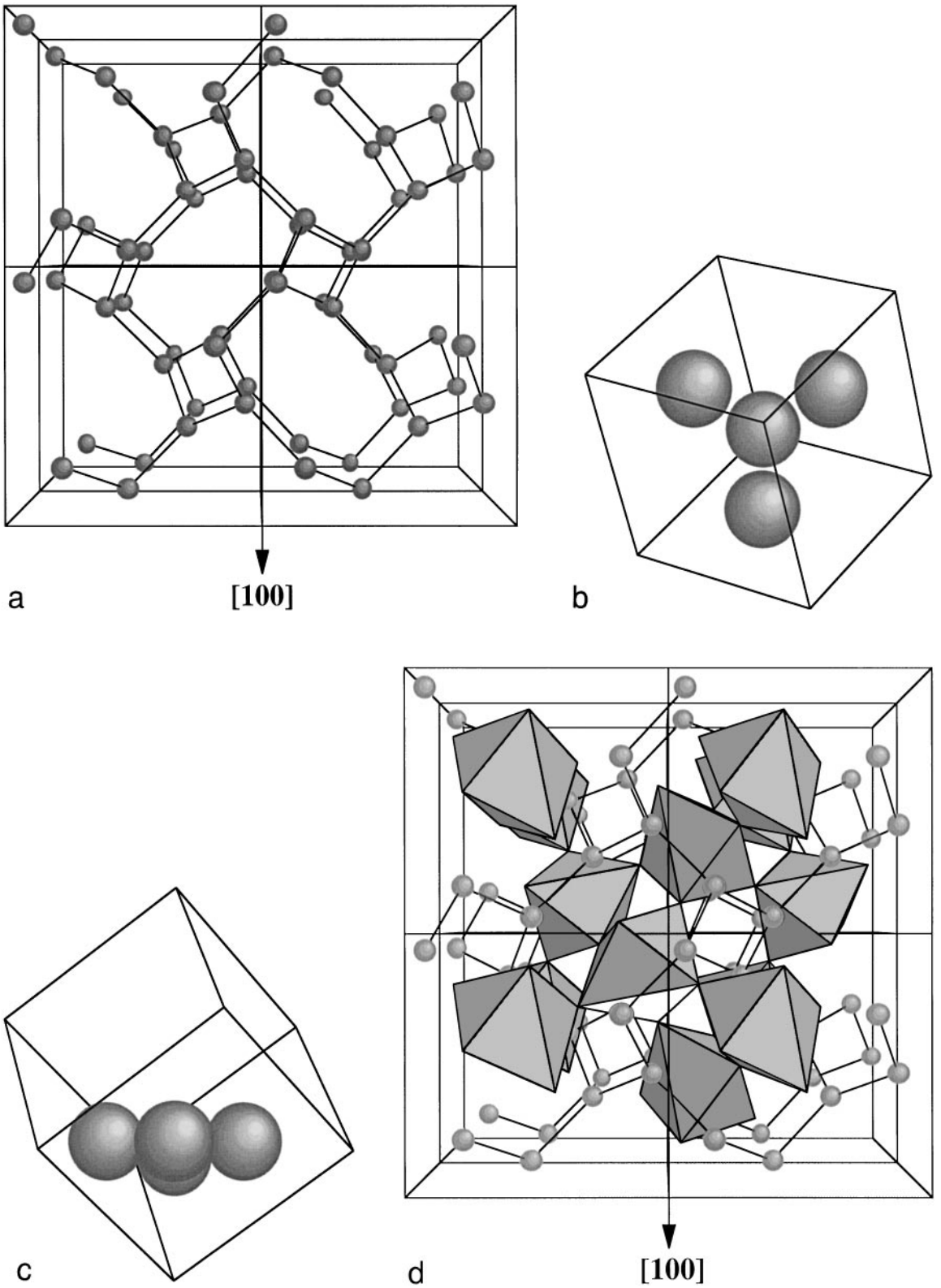

FIG. 8. Representations of the nickel connectivity in the Ni_2Mo_3N structure. (a) shows the "net-like" linkages between the nickel atoms in this intermetallic nitride. (b) and (c) display the triangular arrangement of each nickel atom's three nickel nearest neighbors. Note in (c) that only the three nearest-neighbor atoms are coplanar, with the central nickel atom resting slightly below this plane. The combination of the two interpenetrating lattices in the Ni_2Mo_3N structure is shown in (d).

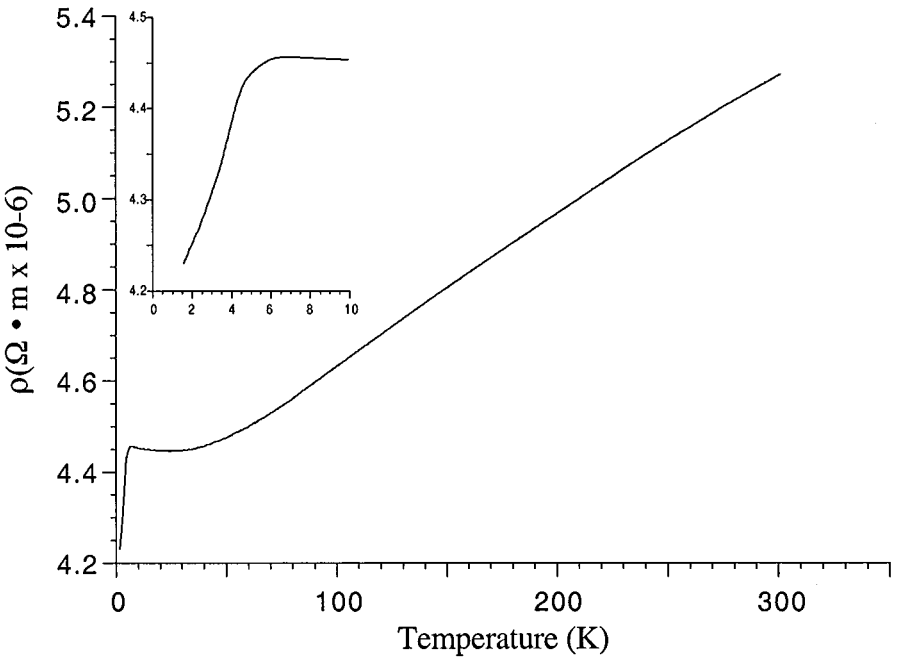

FIG. 9. Resistivity data for Ni_2Mo_3N as a function of temperature. Displayed in the inset is the electrical behavior at low temperatures.

within experimental error θ_b^2 is approximately zero implies that the sublattices are identical, but opposite in spin and Eq. [1] actually reduces to the Curie–Weiss law. From the Curie constant, the effective number of Bohr magnetons per nickel atom (μ_{eff}) was determined to be 1.4(3). The experimental value for metallic nickel beyond its Curie point is 1.61 μ_B, although the value calculated from band theory is 1.25 μ_B, while that for ionic nickel in the $+2$ state is 3.12 μ_B(43). Although the magnetic data for Ni_2Mo_3N is fairly consistent with a two sublattice model, observed bond lengths suggest that metallic, or iternerant electron, magnetic behavior for the nickel atoms should be expected. That is, based on the metallic bonding distances within the nickel net, it may be more appropriate to explain the magnetism observed in Ni_2Mo_3N in terms of its conduction electrons, which we know are available in this compound because of its good metallic conductivity. With this in mind, we are currently reviewing the magnetic and structural data within a band theory framework.

As mentioned previously, differences in the Néel temperature of Ni_2Mo_3N were observed between the electrical conductivity and magnetic susceptibility test samples. To explore this incongruity further, susceptibility measurements were conducted on the 950°C heat treated Ni_2Mo_3N powder. The plot for this material, shown in Fig. 11, displays an antiferromagnetic maxima centered about a temperature of 68.7 K. This peak is much broader than that seen for the 850°C ammonolyzed sample. Broadness in this type of data is generally associated with either low dimensional magnetic ordering or a second-order three-dimensional magnetic phase transition (44). The X-ray diffraction pattern of this material closely resembled that of the 850°C ammonolyzed sample, which was rigorously identified as a mixture of Ni_2Mo_3N and Mo_2N, in a ratio of $\sim 94.3\%$ and $\sim 5.7\%$ by weight, respectively. However, one difference between the two samples alluded to previously is their nitrogen contents. TGA and additional combustion analyses indicated that the 850°C sample was composed of 17.6 at.% nitrogen, whereas the 950°C sample was estimated to contain 15.0 at.% nitrogen. By assuming that the molybdenum nitride impurity in both samples is stoichiometric, the minimum nitrogen content in the Ni_2Mo_3N phase is calculated to be 16.7 at.% for the 850°C sample and 13.4 at.% for the 950°C sample. Compared to the theoretical value of 16.67 at% in Ni_2Mo_3N, the 850°C ternary nitride assumes the ideal nitrogen stoichiometry, which is confirmed by our refinement results, while the 950°C ternary compound is substoichiometric in nitrogen by nearly 20% of the ideal value.

Lattice parameter measurements indicate that the size of Ni_2Mo_3N heat-treated at 950°C is 1.6% smaller in volume than that of the same nitride heat-treated at 850°C, $a_{950°C} = 6.5985(4)$ Å and $a_{850°C} = 6.6340(2)$ Å, which correlates with the calculated nitrogen deficiency in the 950°C sample. This slight contraction in the size of the Ni_2Mo_3N unit cell appears to have a significant effect on the magnetic ordering temperature. Analogous effects on the Curie temperature of the ferromagnetic 2–17 compounds, $Re_2Fe_{17}M_x$ (where Re = rare earth element and M is an interstitial element), have been observed and have been attributed in

part to an increase in the Fe–Fe exchange interactions associated with the change in cell volume (approximately 6–7%) in these materials (45). Similarly, the effect of lattice parameter changes on the Ni–Ni exchange interactions in Ni_2Mo_3N is likely to play a predominant role in the magnetic behavior of this compound, again leading us to believe that a conduction band approach, such as was used for the 2–17 compound (46), is likely to be the most appropriate means of interpreting the magnetic behavior of this compound.

CONCLUSIONS

The crystal structure and the electrical and magnetic properties of the ternary transition metal nitride Ni_2Mo_3N have been investigated by a combination of techniques, including X-ray and neutron diffraction, Rietveld refinement, chemical analyses, four-point resistivity tests, and magnetic susceptibility measurements. This nitride crystallizes in a filled β-manganese structure, which ideally consists of a lattice of corner-sharing Mo_6N octahedra in a five-membered ring arrangement and an interpenetrating net-like lattice of nickel atoms which occupy the pentagonal holes formed by the molybdenum nitride polyhedral rings. Electrical measurements on Ni_2Mo_3N indicate that it is a metallic conductor over a temperature range of 49.8 and 300 K, but displays anomalous behavior below 49.8 K. A sharp decrease in resistivity, indicative of a possible Meissner effect, was observed at 5.9 K, but the test temperature could not be reduced to a point low enough where zero resistivity could be observed. Because of the limited temperature range of the magnetic test equipment, susceptibility measurements on the sample could not be used to confirm this behavior. Since the sample was known to contain ~ 6 wt% Mo_2N, it was not possible to test whether the drop in resistivity is attributable to the Ni_2Mo_3N or the Mo_2N phase. Stoichiometric Ni_2Mo_3N exhibits antiferromagnetic ordering with an ordering temperature of 14.7 K and neutron diffraction conducted on this material at 10 K suggests that the size of the magnetic unit cell matches that of the crystallographic unit cell. Ni_2Mo_3N which is substoichiometric in nitrogen by 20% and has a correspondingly smaller lattice parameter also displays antiferromagnetic ordering, but with a much higher ordering temperature of 68.7 K.

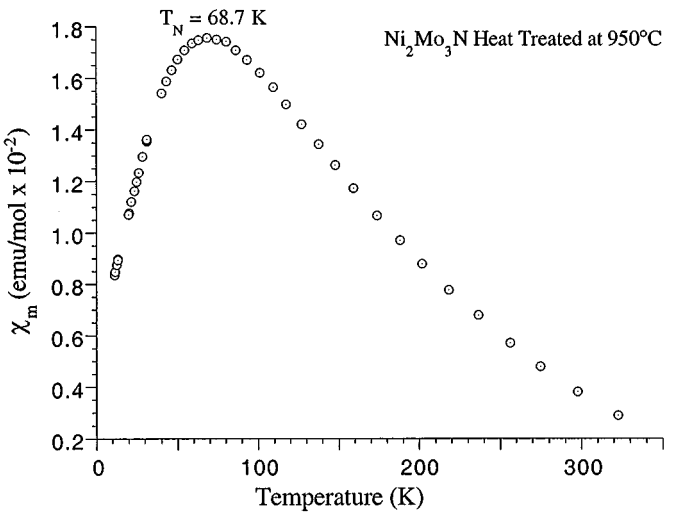

FIG. 11. The molar susceptibility of Ni_2Mo_3N, ammonolyzed at 950°C, as a function of temperature. The Néel temperature is estimated to be 68.7 K.

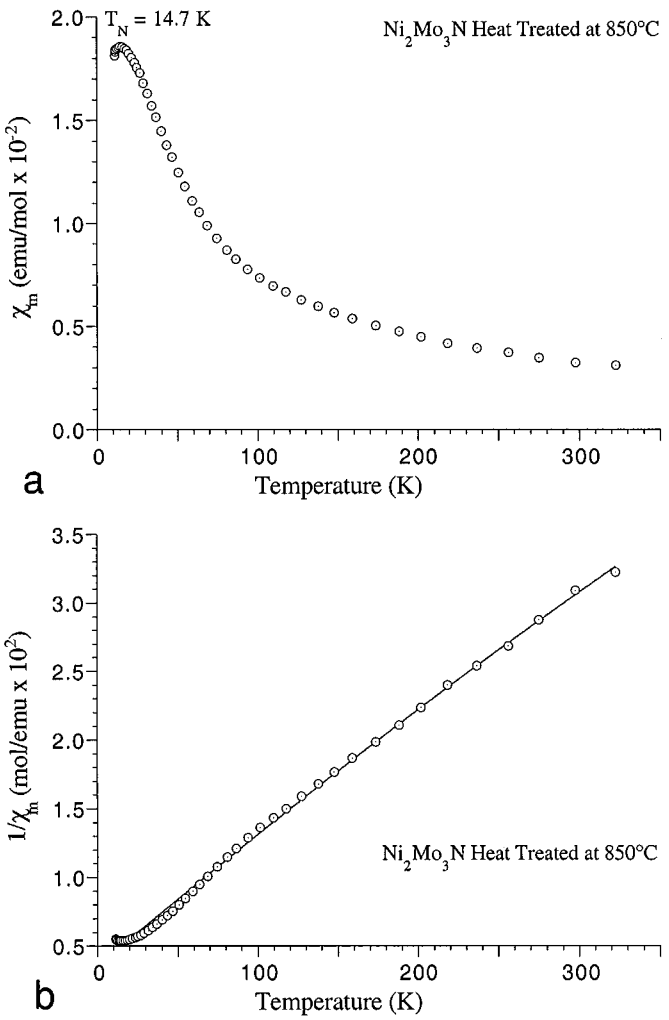

FIG. 10. (a) The molar susceptibility and (b) the inverse molar susceptibility of Ni_2Mo_3N, ammonolyzed at 850°C, as a function of temperature. The solid line shows the fit of the data to Eq. [1].

ACKNOWLEDGMENTS

The authors acknowledge the assistance of Lars Göethe at Stockholm University for preparing the Guinier Hägg data, Björn Lundqvist at the

Royal Institute of Technology in setting up and helping to analyze the four-point conductivity measurements, and Dr. Gunnar Svensson at Stockholm University in conducting the TEM analyses. This work was supported by the National Science Foundation under Grant Nos. CTS-9309073 and CTS-9700343. One of the authors (KSW) also acknowledges the support of the Electrochemical Society in the form of the F. M. Becket Memorial Award to study overseas and the support of the ICCD for crystallography studies on the Ni–Mo–N system. Acknowledgment is also made to Chang Ascending, Taiwan, and Pittsburgh Plate Glass (PPG), Pittsburgh, for partial support of this research.

REFERENCES

1. G. W. Wiener and J. A. Berger, *J. Metals* **7,** 360 (1955).
2. H. Holleck and F. Thümmler, *Monatsh. Chem.* **98,** 133 (1967).
3. J. Grins, P.-O. Kall, and G. J. Svensson, *J. Mater. Chem.* **5,** 571 (1995).
4. D. S. Bem, C. M. Lampe-Onnerud, H. P. Olsen, and H.-C. zur Loye, *Inorg. Chem.* **35,** 581 (1996).
5. H. J. Goldschmidt, *Metallurgia* **1,** 17 (1957).
6. K. Kuo, *J. Metals* **8,** 97 (1956).
7. W. Jeitschko, H. Nowotny, and F. Benesovsky, *Monatsh. Chem.* **94,** 247 (1963).
8. W. Jeitschko, H. Nowotny, and F. Benesovsky, *Monatsh. Chem.* **95,** 1213 (1964).
9. N. Ono, M. Kajihara, and M. Kikuchi, *Metall. Trans. A* **23,** 1389 (1992).
10. M. Kikuchi, M. Kajihara, and K. Frisk, *in* "Proc. Int. Conf. High Nitrogen Steels," p. 63. The Institute of Metals, London, 1989.
11. S. Hertzman, *Metall. Trans. A* **18,** 1767 (1987).
12. K. Frisk, Ph.D. dissertation, Royal Institute of Sweden, Stockholm, Sweden, 1990.
13. D. A. Evans and K. H. Jack, *Acta Cryst.* **10,** 769 (1957).
14. K. M. Nutter, Ph.D. dissertation, University of Newcastle-upon-Tyne, Newcastle, England, 1969.
15. A. J. Carr, P. Korgul, and K. H. Jack, *in* "Proc. Int. Conf. Science of Hard Materials," p. 525. Adam Hilger, Bristol, 1986.
16. P. S. Herle, M. S. Hedge, K. Sooryanarayana, T. N. Guru Row, and G. N. Subbanna, *Inorg. Chem.* **37,** 4128 (1998).
17. K. S. Weil and P. N. Kumta, *J. Solid State Chem.* **128,** 2 (1997).
18. K. S. Weil and P. N. Kumta, *Acta Cryst. C* **53,** 1745 (1997).
19. E. A. Allen, B. J. Brisdon, and G. W. A. Fowles, *J. Chem. Soc.*, 4531 (1964).
20. ASTM D5373-93 (1997), "Standard Test Methods for Instrumental Determination of Carbon, Hydrogen, and Nitrogen in Laboratory Samples of Coal and Coke."
21. K-E. Johansson, T. Palm, and P.-E. Werner, *J. Phys. E* **13,** 1289 (1980).
22. A. Boultif and D. Louer, *J. Appl. Cryst.* **24,** 987 (1991).
23. P.-E. Werner, *Arkiv Kemi* **31,** 513 (1969).
24. J. Rodriguez-Carvajal, M. T. Fernandez-Diaz, and J. L. Martinez, *J. Phys: Cond. Matt.* **3,** 3215 (1991).
25. P. Thompson, D. E. Cox, and J. B. Hastings, *J. Appl. Cryst.* **20,** 79 (1987).
26. R. A. Young, *in* "The Rietveld Method" (R. A. Young, Ed.), Chap. 1. Oxford Univ Press, Oxford, 1993.
27. C. J. Howard, *J. Appl. Cryst.* **15,** 615 (1982).
28. C. Boudias and D. Monceau, *Ca.R.Ine Cristallogr.*, version 3.0 (1989).
29. K. S. Weil and P. N. Kumta, unpublished data.
30. H. Jacobs and E. von Pinkowski, *J. Less-Common Met.* **146,** 147 (1989).
31. P. Höhn, R. Kniep, and A. Rabenau, *Z. Kristallogr.* **196,** 153 (1991).
32. JCPDS-ICDD Powder Diffraction File number 35-787.
33. R. Marchand, *in* "The Chemistry of Transition Metal Carbides and Nitrides" (S. T. Oyama, Ed.), Blackie Acad. Professional, London, 1996.
34. A. Westgren and Phragmen, *Z. Phys.* **33,** 777 (1925).
35. H. Nyman, S. Andersson, B. G. Hyde, and M. O'Keeffe, *J. Solid State Chem.* **26,** 123 (1978).
36. D. S. Bem, C. P. Gibson, and H.-C. zur Loye, *Chem. Mater.* **5,** 397 (1993).
37. A. C. Fraker and H. H. Stadelmaier, *Trans. Met. Soc. AIME* **237,** 214 (1969).
38. J. Johnston, L. E. Toth, K. Kennedy, and E. R. Parker, *Solid State Commun.* **2,** 123 (1964).
39. H. J. Fink, A. C. Thorsen, E. Parker, V. F. Zackay, and L. Toth, *Phys. Rev. A.* **138,** 1170 (1965).
40. L. E. Toth, "Transition Metal Carbides and Nitrides." Academic Press, San Diego, 1971.
41. D. Fruchart, *Physica B* **86–88,** 423 (1977).
42. D. Fruchart and E. F. Bertaut, *J. Phys. Soc. Jpn.* **44,** 781 (1978).
43. R. L. Carlin, *in* "Magnetochemistry." Springer-Verlag, Berlin, 1986.
44. M. E. Fisher, *Philos, Mag.* **97,** 1731 (1962).
45. H. Sun, H. Bo-Ping, L. Hong-shou, and J. M. D. Coey, *Solid State Commun.* **74,** 727 (1990).
46. S. S. Jaswal, Y. G. Ren, and D. J. Sellmyer, *J. Appl. Phys.* **67,** 4564 (1990).